BIOCHEMISTRY
including biophysical chemistry & molecular biology

Article

pubs.acs.org/biochemistry

A Distal Mutation Perturbs Dynamic Amino Acid Networks in Dihydrofolate Reductase

David D. Boehr,[†,§] Jason R. Schnell,[†,∥] Dan McElheny,[†,⊥] Sung-Hun Bae,[†,@] Brendan M. Duggan,[†,#] Stephen J. Benkovic,[‡] H. Jane Dyson,[†] and Peter E. Wright*[,†]

[†]Department of Integrative Structural and Computational Biology and Skaggs Institute for Chemical Biology, The Scripps Research Institute, 10550 North Torrey Pines Road, La Jolla, California 92037, United States

[‡]Department of Chemistry, The Pennsylvania State University, 414 Wartik Laboratory, University Park, Pennsylvania 16802, United States

Supporting Information

ABSTRACT: Correlated networks of amino acids have been proposed to play a fundamental role in allostery and enzyme catalysis. These networks of amino acids can be traced from surface-exposed residues all the way into the active site, and disruption of these networks can decrease enzyme activity. Substitution of the distal Gly121 residue in *Escherichia coli* dihydrofolate reductase results in an up to 200-fold decrease in the hydride transfer rate despite the fact that the residue is located 15 Å from the active-site center. In this study, nuclear magnetic resonance relaxation experiments are used to demonstrate that dynamics on the picosecond to nanosecond and microsecond to millisecond time scales are changed significantly in the G121V mutant of dihydrofolate reductase. In particular, picosecond to nanosecond time scale dynamics are decreased in the FG loop (containing the mutated residue at position 121) and the neighboring active-site loop (the Met20 loop) in the mutant compared to those of the wild-type enzyme, suggesting that these loops are dynamically coupled. Changes in methyl order parameters reveal a pathway by which dynamic perturbations can be propagated more than 25 Å across the protein from the site of mutation. All of the enzyme complexes, including the model Michaelis complex with folate and nicotinamide adenine dinucleotide phosphate bound, assume an occluded ground-state conformation, and we do not observe sampling of a higher-energy closed conformation by ^{15}N R_2 relaxation dispersion experiments. This is highly significant, because it is only in the closed conformation that the cofactor and substrate reactive centers are positioned for reaction. The mutation also impairs microsecond to millisecond time scale fluctuations that have been implicated in the release of product from the wild-type enzyme. Our results are consistent with an important role for Gly121 in controlling protein dynamics critical for enzyme function and further validate the dynamic energy landscape hypothesis of enzyme catalysis.

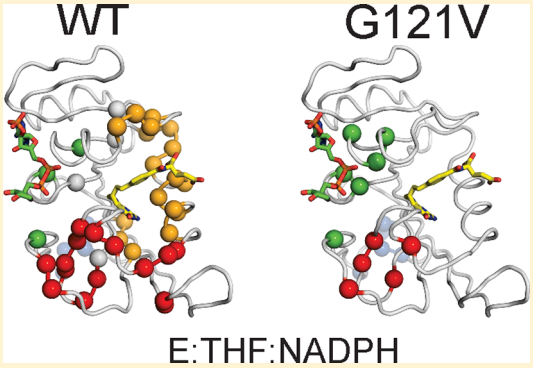

There is now a significant body of evidence supporting a functional role for protein dynamics in biologically important processes such as protein−protein interactions, allosteric regulation, and enzyme catalysis.[1−8] These studies suggest that protein motions can be directed toward a functional purpose (e.g., capture or release of a ligand). It has been suggested that coupled networks of amino acids exist in proteins such that motions in distant regions can influence events at a functional site.[3,7,9−13] It has also been shown that disruption of these proposed networks leads to severe impairment of protein function,[3,8] suggesting new mechanisms of allostery whereby changes in global structure and/or protein dynamics can significantly influence biological activity, even in monomeric or traditionally "nonallosteric" proteins.[14−18] These insights offer additional complexities to protein engineering and new opportunities for drug design.

One of the enzymes in which coupled networks of protein motion have been proposed to play a major role in catalytic function is *Escherichia coli* dihydrofolate reductase (DHFR).[9,12,19−22] DHFR is a small (18 kDa) enzyme that catalyzes the reduction of folate (FOL) to dihydrofolate (DHF) and dihydrofolate (its physiological substrate) to tetrahydrofolate (THF) using the cofactor NADPH.[23] The rate-limiting step in the steady-state catalytic cycle is the release of product THF, which is coupled to rebinding of NADPH to the enzyme.[24] Structural and kinetic studies suggest that control over substrate and cofactor binding is mediated by several flexible loops that surround the active site.[25−28] The loops are termed the Met20 (residues 9−24), FG (residues 116−132), and GH (residues 142−150) loops (Figure 1). These loops assume three distinct conformations in the crystalline state, denoted occluded, closed, and open,[25] although only the

Received: May 2, 2013
Revised: June 10, 2013
Published: June 11, 2013

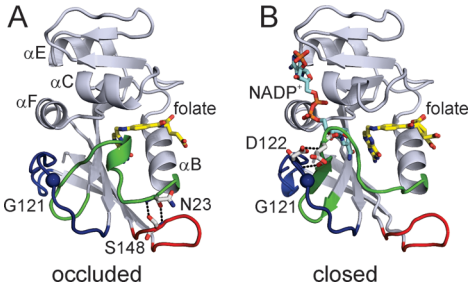

Figure 1. Structures representing the (A) occluded (PDB entry 1RX7)[25] and (B) closed loop (PDB entry 1RX2)[25] conformations of *E. coli* DHFR. The active-site loops are colored green (Met20), blue (FG), and red (GH). Residues involved in hydrogen bonding interactions between these loops are shown as sticks and labeled. Hydrogen bonds that stabilize the different loop conformations are indicated with dashed lines. In the occluded conformation of the Met20 loop (A), hydrogen bonds are formed between Asn23 in the Met20 loop and Ser148 in the FG loop. In the closed conformation of the Met20 loop (B), hydrogen bonds are formed between Asp122 in the FG loop and Gly15 and Glu17 in the Met20 loop. This figure was prepared using PyMOL.[99]

occluded and closed loop conformations appear to be significantly populated in solution.[29] In product complexes, the Met20 loop is occluded, with the central region (residues Met16 and Glu17) flipped into the cofactor binding pocket such that the nicotinamide ring is sterically occluded from binding. However, when the nicotinamide ring binds in the active site, Met16 and Glu17 move out of the binding pocket, residues Met16–Ala19 adopt a type III′ β-hairpin, and the side chains of Asn18 and Met20 pack over the pterin ring to form the closed conformation. Only the closed conformation allows proximal positioning of the cofactor and substrate reactive centers, and therefore, it is the closed conformation that must be adopted in the Michaelis complex.[25,29] The occluded and closed Met20 loop conformations are stabilized by unique networks of hydrogen bonds to the GH and FG loops, respectively.

On the basis of mixed quantum mechanical/classical molecular dynamics simulations (QMMM), it has been proposed that a network of coupled promoting motions, involving amino acid residues in the active site and on the exterior of the protein, is important for DHFR catalysis.[9] In particular, Gly121 and Asp122 in the FG loop appear to participate in a network of correlated protein motions that act to compress the reaction coordinate and stabilize the transition state.[9,19−21] Consistent with this hypothesis, Gly121 and Asp122 mutants exhibit significantly decreased hydride transfer rates.[26,27,30−34] For example, mutation of Gly121 to Val results in a 40-fold decrease in NADPH binding affinity and a 200-fold decrease in the hydride transfer rate, despite the fact that Gly121 is located ∼15 Å from the active site[34] (Figure 1). In addition, the G121V mutation results in a 7-fold decrease in the rate of product release.[34] Moreover, enzymes with double and triple mutations involving Gly121 and other proposed members of the network (e.g., Met42) showed synergistic decreases in hydride transfer rates, suggesting that the amino acid residues in the network are kinetically and thermodynamically coupled.[21,35] Both molecular dynamics simulations[21,36] and experimental kinetic isotope effects suggest different gating motions or conformational sampling between the WT and mutant enzyme.[37−39]

These results are especially interesting in light of the fact that Gly121 appears to be the most flexible residue in the enzyme. Previous NMR relaxation studies of the backbone dynamics of DHFR identified large amplitude motions on the nanosecond time scale for Gly121 and other residues in the FG loop.[40−42] NMR R_2 relaxation dispersion experiments have also shown that Gly121 is conformationally mobile on the microsecond to millisecond time scale for most complexes of DHFR.[43,44] These results raise questions about the role of flexibility and protein motion in DHFR catalysis and, specifically, the role of Gly121 in the catalytic cycle of DHFR.

To further explore the relationship between catalysis and protein dynamics in DHFR, we used NMR relaxation experiments to study protein dynamics on the picosecond to millisecond time scales for four complexes of G121V DHFR – E:FOL:NADP$^+$, a model for the Michaelis complex (E:DHF:NADPH); E:FOL, a model for the binary product complex (E:THF); and the two product ternary complexes, E:THF:NADP$^+$ and E:THF:NADPH. The largest motional differences between WT and G121V DHFR on the picosecond to nanosecond time scale are for residues located in the FG and Met20 loops, providing evidence that motions in the active-site loops are coupled. These changes in dynamics are propagated more than 25 Å across the protein to the adenosine-binding domain. Moreover, in all four complexes, the G121V enzyme populates an occluded ground state[29] and does not appear to significantly sample the catalytically competent closed conformation on the microsecond to millisecond time scale (population of <1% of the conformation ensemble). These results help to explain the differences in ligand affinities and hydride transfer rates between WT and G121V enzymes and serve as a further validation of the dynamic energy landscape hypothesis of enzyme catalysis.[8,45,46]

MATERIALS AND METHODS

Sample Preparation. WT and G121V DHFR were overexpressed and purified as described previously.[26,40,45] Samples for resonance assignments consisted of an ∼1.0−1.5 mM solution of G121V DHFR uniformly labeled with ^{15}N and ^{13}C or ^{2}H, ^{15}N, and ^{13}C. Samples for R_1, R_2, and heteronuclear NOE experiments consisted of ∼1.5 mM protein uniformly labeled with ^{15}N. R_2 relaxation dispersion experiments were performed with 1 mM uniformly ^{2}H- and ^{15}N-labeled DHFR.

Samples for the measurement of methyl ^{2}H relaxation consisted of a 2.5−3.0 mM solution of G121V protein uniformly labeled with ^{15}N and ^{13}C, and with partial random deuteration at all nonexchangeable proton sites. Deuteration to ∼45% results in a large fraction of methyls with a single deuterium spin ($^{13}CH_2^2H$) and was achieved by growth of transformed *E. coli* BL21-DE3 cells on 65% D_2O. The extent of deuteration was estimated by matrix-assisted laser desorption ionization mass spectrometry.

NMR samples for E:FOL and E:FOL:NADP$^+$ complexes were prepared in argon-flushed buffer (pH 6.8) containing 50 mM potassium phosphate, 100 mM KCl, and 1 mM DTT and stored in amberized tubes sealed with a septum. FOL and NADP$^+$ were added to 6- and 10-fold excesses over protein, respectively. THF and NADPH are more susceptible to oxidation; therefore, the buffer was thoroughly degassed through freeze–pump–thaw cycles using a vacuum apparatus, and ascorbic acid was added to act as an oxygen scavenger. The final samples for the E:THF:NADP$^+$ or E:THF:NADPH complex contained 1 mM DHFR, 10 mM NADP$^+$/NADPH,

dx.doi.org/10.1021/bi400563c | *Biochemistry* 2013, 52, 4605−4619

6 mM THF, 1 mM DTT, 25 mM KCl, and 10% D_2O in 70 mM KP_i (pH 7.6). The samples were placed in amberized NMR tubes, subjected to vacuum again, overlaid with argon, and flame-sealed.

Resonance Assignments. Backbone amide assignments for the G121V complexes were determined using either standard[47−49] or deuterium-decoupled[50] versions of HNCA and HNCACB for ^{13}C- and ^{15}N-labeled and ^{2}H-, ^{13}C-, and ^{15}N-labeled mutant proteins, respectively. In some cases (E:FOL and E:FOL:$NADP^+$), additional experiments, including HN(CO)CA, HN(CO)CACB, and/or CBCA(CO)NH, were used to confirm the assignments. Methyl resonances for the E:FOL complex were assigned from three-dimensional ^{15}N TOCSY-HSQC[51] and (H)C(CO)NH/H(CCO)NH spectra.[52]

***R_1*, *R_2*, and Heteronuclear NOE.** ^{15}N relaxation data for the WT and G121V E:FOL complexes were recorded at 306.4 K at three fields using Bruker Avance 500 MHz, DRX 600 MHz, and DMX 750 MHz spectrometers (Figure S1 of the Supporting Information). The pulse sequences closely followed those of Farrow et al.[53] with sensitivity enhancement and coherence selection via pulsed field gradients. NMR samples of the two complexes were made fresh within a month of each other using the same folate stock, and relaxation parameters were collected back to back on the same spectrometers to ensure the smallest amount of sample and spectrometer variability. The choices of delays in the R_1 and R_2 experiments were based on the two-delay Cramer−Rao approach[54] in which the shortest experimentally accessible delay is recorded along with a second delay at 1.3 times the relaxation time, taken as the trimmed mean (T_{mean}) for all residues. Optimal delays were chosen on the basis of preliminary measurements in which the full decay was sampled. The R_1 experiments were recorded with a short delay of 10 ms and a long delay ($\sim 1.3T_{mean}$) of 770 ms (500 MHz), 1000 ms (600 MHz), or 1606 ms (750 MHz). The R_2 measurements were recorded with a short delay of 4 ms and a long delay ($\sim 1.3T_{mean}$) of 120 ms (500 and 600 MHz) or 108 ms (750 MHz). Three (two) duplicates at the short delay and five (four) duplicates at the long delay at 500 and 750 MHz (600 MHz) allowed direct estimation of the uncertainty in the peak intensity on a residue-by-residue basis. The R_1 and R_2 rates were determined from a two-parameter exponential fit to the peak heights using CurveFit.[55,56] R_2 data obtained previously for the same WT sample at 600 MHz using a traditional sampling scheme with 10 delays spaced between the shortest attainable delay to roughly $2.5T_{mean}$ were compared to R_2 data measured using the Cramer−Rao method. The R_2 values derived from the two sampling schemes were very similar. The average R_2 values and standard deviations were 10.66 ± 1.16 and 10.73 ± 1.26 s^{-1}, and the range of R_2 values was 6.10−16.60 and 5.82−16.66 s^{-1} for traditional and Cramer−Rao sampling schemes, respectively.

The $\{^1H\}-^{15}N$ NOE was recorded five (600 MHz) or six (500 and 750 MHz) times with a saturation period consisting of 120° ^1H pulses spaced 18 ms apart for a total of 3.0 s.[57] The saturated and unsaturated spectra were recorded in an interleaved manner to minimize systematic errors. A relaxation delay of 2.6 s was used for all ^{15}N relaxation experiments.

COPED Analysis. An accurate description of the internal motions requires that deviations from isotropic molecular tumbling be taken into account.[58] Previous work has identified a small degree of anisotropic molecular rotation in *E. coli* DHFR that, if neglected, can lead to erroneous fitting of exchange terms (R_{ex}).[59] Care must be taken that residues with genuine exchange terms or large amplitude internal motions are not included in the initial description of the molecular diffusion parameters.[60] With this in mind, the COPED approach[59] was used to determine the diffusion tensor and rotational correlation time τ_m through a comparison of the experimental local diffusion coefficients derived from relaxation data and the diffusion coefficients predicted from a hydrodynamic model. In this way, residues with significant contributions to relaxation rates from picosecond to nanosecond or microsecond to millisecond motions were identified and excluded from the initial calculations of the molecular diffusion parameters. Predicted local diffusion coefficients $[D_{i(pred)}]$ were calculated using the in-house program MASH (written by I. Radhakrishnan), which incorporates the HYDRO suite of programs.[61] The protein was modeled as a set of beads with a radius of 3.09−3.11 Å centered on the Cα atoms. The exact bead radius was chosen to minimize the error function $\chi^2 = [D_{i(exp)} - D_{i(pred)}]/\sigma^2$, where σ is the uncertainty in $D_{i(exp)}$. The experimental local diffusion coefficients were calculated from local correlation times estimated from the R_2/R_1 ratio using the program tmest.[62] Residues with a positive or negative deviation from $D_{i(pred)}$ and a χ^2 of >6 at either 500 or 600 MHz were identified as undergoing picosecond to nanosecond or microsecond to millisecond internal motions, respectively, and excluded from determination of the initial diffusion tensor. These residues were later reintroduced for the determination of model-free parameters. As shown in Table S1 of the Supporting Information, the lists of excluded residues are similar for WT and G121V DHFR. However, FG loop residues 120−122, which are excluded for the WT because of picosecond to nanosecond motions, no longer exhibit these motions in G121V DHFR. Instead, residues 119 and 122 are excluded because of predicted microsecond to millisecond motions. Residues exhibiting a $\{^1H\}-^{15}N$ NOE of <0.65 were also excluded from the calculation of the molecular diffusion parameters. The initial estimates of τ_m based on the ^{15}N R_2/R_1 ratios of the retained residues were 8.72 and 8.64 ns for WT and G121V DHFR, respectively. Final τ_m values optimized using the model-free results (Table S2 of the Supporting Information) differed only slightly. The program quadric_diffusion was used to estimate $D_{\parallel}/D_{\perp}$ and rotate the crystal structure along the principal component of the diffusion tensor.

Anisotropic Model-Free Analysis. The relaxation data sets for the WT and G121V E:FOL complexes were analyzed independently using an axially symmetric diffusion tensor and ModelFree version 4.15. Backbone amide vector orientations determined from the crystal structure of DHFR in complex with folate (PDB entry 1RX7)[25] were used for both WT and G121V DHFR (see Results). Although an N−H bond length of 1.04 Å and a ^{15}N CSA of −160 ppm may be more physically reasonable,[63,64] the combination of 1.02 Å and −172 ppm was used in this study to facilitate comparison with earlier work. With these parameters, S^2 values reflect both librational motions of the peptide plane and quantum mechanical zero-point motions. The CSA for the $^{15}N^{\varepsilon}$ atom in the tryptophan indole ring was set to −126 ppm. For each complex, the relaxation data at multiple fields were fit simultaneously using the extended Lipari−Szabo formalism.[65] The appropriate dynamic model for each residue (model 1, S^2; model 2, S^2 and τ_e; model 3, S^2 and R_{ex}; model 4, S^2, τ_e, and R_{ex}; model 5, S_f^2, S_s^2, and τ_e) was selected with an in-house program using the Bayesian information criterion for model selection (Table S3 of the Supporting Information).[66−68]

dx.doi.org/10.1021/bi400563c | *Biochemistry* 2013, 52, 4605−4619

Table 1. Kinetic and Thermodynamic Fitting Parameters for WT and G121V DHFR ^{15}N R_2 Relaxation Dispersion Curves

	WT[a,b]						G121V[a]					
	cluster 1, active site[c]			cluster 2, C-terminal region			cluster 1, active site[c]			cluster 2, C-terminal region		
	p_b	k_{AB} (s^{-1})	k_{BA} (s^{-1})	p_b	k_{AB} (s^{-1})	k_{BA} (s^{-1})	p_b	k_{AB} (s^{-1})	k_{BA} (s^{-1})	p_b	k_{AB} (s^{-1})	k_{BA} (s^{-1})
E:F												
306 K	0.030	16.1	521	0.031	14.9	465	0.017[d]	11.0	624	0.034	46.8	1320
E:F:N^+												
303 K	0.043	20.4	457	0.038	37.8	972	0.055	28.1	484	0.032	29.8	900
306 K	0.055	30.5	524	0.037	45.1	1234	0.060	32.8	517	0.036	32.8	871
309 K	0.072	43.0	552	nd[e]	nd[e]	nd[e]	0.062	40.0	605	nd[e]	nd[e]	nd[e]
312 K	0.082	53.2	598	nd[e]	nd[e]	nd[e]	0.069	61.5	833	nd[e]	nd[e]	nd[e]
E:T:N^+												
300 K	0.014[f] (0.030)	18.5[f] (50.8)	1280[f] (1650)	0.022	12.4	538	0.069	47.6	644	0.024	17.2	714
E:T:NH												
300 K	0.025	18.5	734	0.018	11.4	610	nd[g]	nd[g]	nd[g]	nd[g]	nd[g]	nd[g]
305 K	nd[g]	nd[g]	nd[g]	nd[g]	nd[g]	nd[g]	0.085	60.3	647	0.026	18.1	687

[a]Uncertainties in the measurements are listed in Table S5 of the Supporting Information. [b]Data for the WT complexes taken from ref 77 for E:FOL, ref 43 for E:FOL:NADP$^+$, ref 45 and unpublished work of D. D. Boehr for E:THF:NADP$^+$, and ref 45 for E:THF:NADPH. [c]The location of the residues showing conformational exchange in the "active site" (including the active-site loops, cofactor-binding cleft, and/or substrate/product binding pocket) depends heavily on the specific complex (see ref 45 and Figure 7). [d]Residues in the cofactor binding site were excluded from the cluster 1 fit (see the text). [e]Not determined. Conformational exchange is apparent but could not be appropriately fit to k_{ex} and/or p_Ap_B. [f]There are three regions of protein dynamics in the WT E:THF:NADP$^+$ complex that have different k_{ex} and p_Ap_B values: the active-site loops, the cofactor-binding cleft, and the C-terminal associated region. The k_{ex} and p_Ap_B values for the cofactor-binding cleft are given in parentheses. [g]Not determined. Data for the WT or G121V complex were not collected at this temperature.

^2H Methyl Side Chain Relaxation. The dynamics of methyl-containing side chains in the G121V E:FOL complex were probed using quadrupolar ^2H relaxation. Relaxation data sets were recorded on Bruker DRX spectrometers operating at ^1H frequencies of 600 and 800 MHz (92 and 123 MHz for ^2H, respectively) using published pulse sequences.[69] Because of a large variation in rates, the two-delay Cramer–Rao method for sampling the decay could not be applied. The $R_1(I_zC_zD_z)$ experiments were recorded with delays of 0.05*, 4, 14, 20, 27, 35*, 44, 64, and 75* ms. The $R_{1\rho}(I_zC_zD_y)$ experiments were recorded with delays of 0.25*, 2, 3.5, 5*, 7, 9, 14*, 17, and 28 ms. The asterisks denote delays at which data were collected in duplicate for the estimation of peak uncertainty. The contribution from spin flips in neighboring protons $R_1(I_zC_z)$ was measured using delays of 0.135*, 11, 30, 50, 80*, 110, 140, 170, and 210* ms and subtracted from the observed deuterium relaxation rates to yield $R_1(^2H)$ and $R_2(^2H)$. All relaxation rates were determined from a two-parameter fit to peak heights using CurveFit.[70] Data points with intensities less than twice the spectral noise were excluded from the fit.[71]

^2H relaxation rates were fit to model-free parameters S_{axis}^2 and τ_e, where S_{axis}^2 reflects motion about the vector between the methyl carbon and the adjacent bonded carbon. S_{axis}^2 is derived from S^2 scaled by $[(3\cos^2\theta - 1)/2]^2$ to remove the contribution from free methyl rotation, where θ is the angle between the $C-C_{methyl}$ bond and the $C_{methyl}-^2H$ bond (109.5°). Fitting was accomplished using ModelFree with the appropriate equations for ^2H quadrupolar relaxation[72] and with the quadrupolar coupling constant (e^2qQ/h) set to 167 kHz.[73] Rotational correlation times were estimated from the ratio of backbone amide ^{15}N relaxation rates R_1 and R_2[74] collected for the same samples. The methyl model-free parameters are summarized in Table S4 of the Supporting Information.

^{15}N R_2 Relaxation Dispersion. ^{15}N R_2 dispersion experiments were performed for G121V E:FOL, E:FOL:NADP$^+$, E:THF:NADP$^+$, and E:THF:NADPH complexes at ^1H spectrometer frequencies of 500 and 800 MHz using constant-time relaxation-compensated CPMG (Carr–Purcell–Meiboom–Gill) pulse sequences.[43,75] The total relaxation time was 40 ms for the E:FOL:NADP$^+$, E:THF:NADP$^+$, and E:THF:NADPH complexes and 80 ms for the E:FOL complex. The R_2 relaxation dispersion data were fit simultaneously at the two frequencies using the in-house computer program GLOVE with the following series of equations describing conformational exchange between two sites, A and B:

$$R_2(1/\tau_{CP}) = R_2^0 + \frac{1}{2}\left\{k_{ex} - \frac{1}{\tau_{CP}}\cosh^{-1}[D_+\cosh(\eta_+) - D_-\cos(\eta_-)]\right\} \quad (1)$$

in which

$$D_\pm = \frac{1}{2}\left[\pm 1 + \frac{\psi + 2\Delta\omega^2}{(\psi^2 + \zeta^2)^{1/2}}\right] \quad (2)$$

$$\eta_\pm = \frac{\tau_{CP}}{\sqrt{2}}[\pm\psi + (\psi^2 + \zeta^2)^{1/2}]^{1/2} \quad (3)$$

where $\psi = k_{ex}^2 - \Delta\omega^2$, $\zeta = -2\Delta\omega k_{ex}(p_A - p_B)$, τ_{CP} is the time between successive 180° pulses in the CPMG pulse train, R_2^0 is the R_2 relaxation rate in the absence of conformational exchange, p_A and p_B are the populations of the ground- and excited-state conformations, respectively ($p_A + p_B = 1$), and $\Delta\omega$ is the chemical shift difference between substates A and B. Rate constants for the ground-to-excited-state transition (k_{AB}) and the excited-to-ground-state transition (k_{BA}) can be determined by p_Bk_{ex} and p_Ak_{ex}, respectively. Residues generally fit in one of two clusters, one containing residues in the active-site loops and/or the substrate, product, or cofactor binding sites and the other consisting of a small cluster of residues near the C-terminus (residues 129–134 and 157–159). Each cluster was fit with global k_{ex} and p_Ap_B values while allowing $\Delta\omega$ values to vary for each residue. The clusters showed significantly different

dx.doi.org/10.1021/bi400563c | Biochemistry 2013, 52, 4605–4619

p_B, k_{AB}, and k_{BA} values (Table 1) (k_{ex} and $p_A p_B$ values are shown in Table S5 of the Supporting Information). The sign for $\Delta\omega$ was determined by comparing HSQC and HMQC spectra;[76] $\Delta\omega$ values are listed in Table S6 of the Supporting Information.

Temperature Dependence of Microsecond to Millisecond Time Scale Dynamics. The enthalpy (ΔH) and entropy ($-T\Delta S$) energy differences between the excited- and ground-state conformations were estimated from the temperature dependence of the conformational exchange equilibrium constant using van't Hoff analysis:

$$\ln K = -\Delta H/RT + \Delta S/R \quad (4)$$

where K is equal to k_{BA}/k_{AB}. Reported errors are based on jackknife simulations.[43,45] The activation barriers were estimated using transition-state theory:

$$k = (k_B T/h)e^{\Delta S^{\ddagger}/R}e^{-\Delta H^{\ddagger}/RT} \quad (5)$$

where k is the rate constant from R_2 relaxation dispersion (k_{AB}), k_B is Boltzmann's constant, h is Planck's constant, R is the universal gas constant, T is the temperature, $\Delta S^{\ddagger}$ is the entropy of activation, and $\Delta H^{\ddagger}$ is the enthalpy of activation.

RESULTS

Chemical Shift Differences between WT and G121V Complexes. Differences in backbone amide chemical shifts between the WT and G121V DHFR complexes are shown in Figure 2. For the E:FOL, E:THF:NADP$^+$, and E:THF:NADPH complexes, the $^1H^N$ and ^{15}N chemical shift differences between WT and G121V complexes are small for most residues (Figure 2A,C,D), indicating that the G121V and WT enzymes adopt the same occluded conformation. Not surprisingly, residues in the FG loop near the site of mutation show large changes in chemical shift, while small chemical shift changes are observed

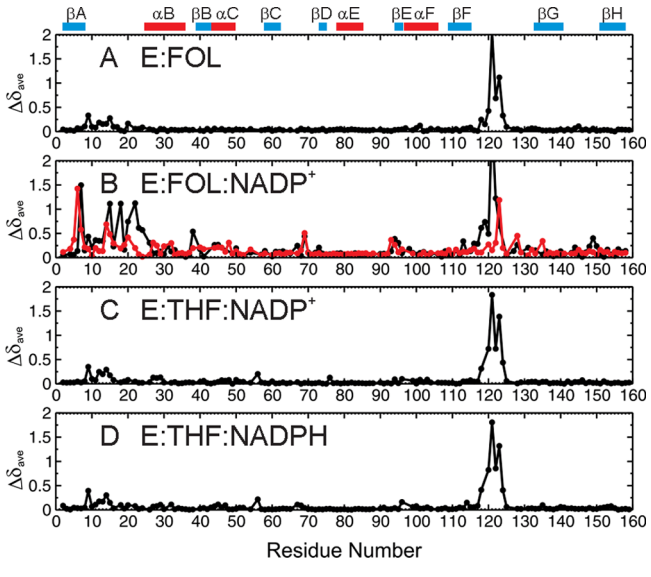

Figure 2. Backbone amide $^1H^N$ and ^{15}N chemical shift differences between WT and G121V DHFR complexes (A) E:FOL, (B) E:FOL:NADP$^+$, (C) E:THF:NADP$^+$, and (D) E:THF:NADPH. The weighted average shift difference ($\Delta\delta_{ave}$) for each residue was calculated as $[(\Delta\delta_H)^2 + (\Delta\delta_N/5)^2]^{1/2}$, where $\Delta\delta_H$ or $\Delta\delta_N$ is δ(G121V) − δ(WT).[100] For E:FOL:NADP$^+$ (B), the black line is a comparison between G121V E:FOL:NADP$^+$ and WT E:FOL:NADP$^+$ complexes and the red line is a comparison between G121V E:FOL:NADP$^+$ and G121V E:THF:NADP$^+$ complexes.

for some residues in the Met20 loop (Ala9, Val10, Arg12, Val13, Ile14, and Gly15), indicative of the subtle adjustment of the backbone to accommodate the bulky Val121 side chain. In contrast to the WT E:FOL:NADP$^+$ complex, which adopts a closed Met20 loop conformation, the E:FOL:NADP$^+$ complex of the G121V mutant remains occluded. With the exception of Ala7, which hydrogen bonds differently with folate and THF,[29] only small chemical shift differences are observed between the E:FOL:NADP$^+$ complex and the occluded E:THF:NADP$^+$ complex of G121V (Figure 2B, red curve). In contrast, there are large differences in chemical shifts for residues throughout the Met20 loop (residues 9−24) between the closed WT E:FOL:NADP$^+$ complex and the occluded G121V E:FOL:NADP$^+$ complex (Figure 2B).

Backbone Picosecond to Nanosecond Time Scale Motions in the G121V E:FOL Complex. The picosecond to nanosecond time scale dynamics of DHFR depend primarily on the backbone conformation,[42] whereas the microsecond to millisecond time scale dynamics are highly ligand specific.[45,77] Backbone amide and tryptophan imino ^{15}N R_1 and R_2 relaxation rates and $\{^1H\}-^{15}N$ NOEs were acquired under identical conditions for the E:FOL complexes of WT and G121V DHFR, both of which adopt occluded ground-state conformations (Figure S1 of the Supporting Information).

After acquisition of the R_1, R_2, and heteronuclear NOE data reported in this paper, Ferrage et al.[78] demonstrated that systematic errors in the magnitude of the NOE can result from the use of a 120° flip angle for ^1H irradiation. On the basis of simulations by Ferrage et al., the measured rotational correlation time of DHFR (~8.6 ns), and the 18 ms spacing between successive 120° pulses in our experiments, we estimate that any errors introduced would be smaller than the uncertainties in the NOE measurements for residues with S^2 values of ≥0.7. For residues in flexible loops, with S^2 values of <0.7, systematic errors could occur in τ_e; however, S^2 values are much more robust and are influenced only slightly by the choice of flip angle.[78] In our analysis of data for residues in flexible loops, differences in dynamics between WT and G121V DHFR were considered to be significant only if a substantial difference was observed in the order parameters ($\Delta S^2 = 0.06 - 0.18$). Further, the relaxation data for the WT and G121V complexes were acquired under identical conditions, and residues that differ in S^2 and τ_e can thus be identified with a high degree of confidence, even if the absolute magnitude of τ_e for residues in flexible loops is subject to systematic error.

Anisotropic model-free analysis[65,79,80] was performed using $^1H-^{15}N$ bond orientations determined from the crystal structure of WT DHFR bound to folate (PDB entry 1RX7) for both WT and G121V relaxation data sets. Use of the WT crystal structure to model anisotropic tumbling of G121V is justified because the available NMR data indicate no large scale structural changes resulting from the mutation. First, large chemical shift differences resulting from the mutation are localized to regions immediately adjacent to the mutation site (Figure 2A). Second, the relationship between the predicted and experimental diffusion coefficients is similar, indicating a comparable rotational correlation time and degree of anisotropy (Figure S2 of the Supporting Information). The final overall diffusion parameters calculated from the model-free results confirm that the structures are very similar (Table S2 of the Supporting Information). Third, it has been shown that only modest changes in the circular dichroism spectra of G121V are observed, and the thermodynamics of urea and

dx.doi.org/10.1021/bi400563c | Biochemistry 2013, 52, 4605−4619

thermal denaturation are similar.[31] Finally, the backbone conformations of Gly121 in the available X-ray structures of the WT E:FOL and E:FOL:NADP$^+$ complexes are in the region of conformational space that is allowed for valine, suggesting that a valine substitution can be accommodated without a significant change in backbone conformation.

Model-free analysis of the ^{15}N relaxation data (Figure 3) shows that backbone amide and tryptophan imino motions in

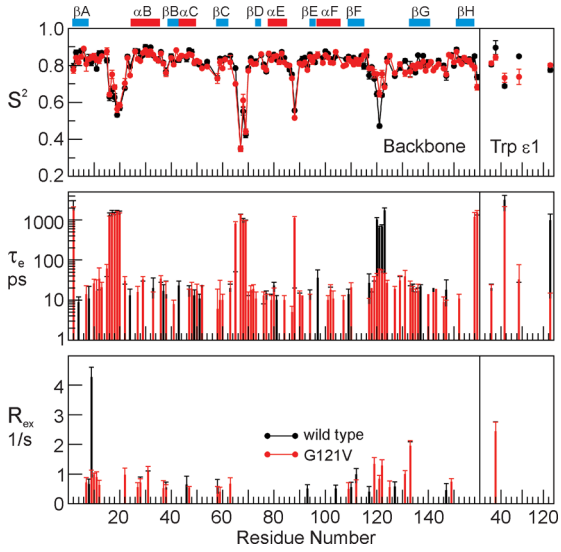

Figure 3. Backbone amide and tryptophan imino model-free parameters S^2, τ_e, and R_{ex} for the WT (black) and G121V (red) E:FOL complexes extracted from fits to data at 500 and 600 MHz. Values for R_{ex} are reported for 600 MHz.

the WT and G121V E:FOL complexes are similar. In both complexes, select residues in the Met20 loop (residues 16−20), the adenosine-binding loop (residues 67−69), and the hinge region (residue 88) have lower than average S^2 and nanosecond τ_e values. Not surprisingly, the largest differences in dynamics between WT and G121V occur near the site of mutation in the FG loop (residues 119−123), where the substitution of the bulky valine results in an increase in S^2 and the introduction of R_{ex} terms. The average backbone S^2 values of residues 120 and 122 increase from 0.64 to 0.75 upon mutation, while the S^2 for residue 121 increases from 0.47 (Gly121) to 0.65 (Val121). Motions of residues 120−123 that are on the order of 0.7−1.8 ns in the WT complex are on the picosecond time scale in G121V (40−50 ps). Thus, substitution of Gly121 with Val causes a decrease in the amplitude of backbone motions in this part of the FG loop and a shift to a faster time scale. The G121V substitution also affects the backbone dynamics of Met20 loop residues, with significant increases in S^2 for residues 11, 15, 17, and 18 (Figure 3).

Interestingly, there are also changes in the backbone amide relaxation of Gln65 or Thr68, located in the CD loop more than 25 Å from the site of the mutation. Gln65 in G121V shows a decrease in S^2 and new nanosecond time scale motions (Figure 3). The locations of these changes are shown on the structure of DHFR in Figure 4. In contrast, the backbone S^2 for Thr68 is increased slightly in the mutant. The occurrence of long-range communication between the active-site loops in the major subdomain and the CD loop has been suggested previously on the basis of both experimental[81] and theoretical studies.[82,83]

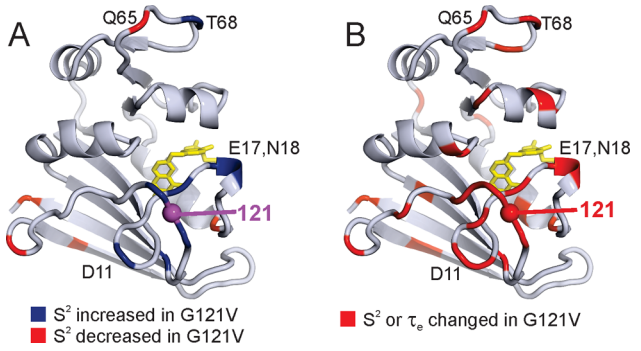

Figure 4. Changes in dynamics in the G121V E:FOL complex, mapped onto the DHFR structure (PDB entry 1RX7).[25] (A) Change in backbone amide S^2 values between the WT and G121V E:FOL binary complexes. Blue denotes an increase in S^2 showing restriction of picosecond to nanosecond backbone motion in the mutant and red a decreased S^2, indicating an increased amplitude of backbone motion in the mutant. (B) Location of residues that show changes in amplitude (S^2) and/or time scale (τ_e) of picosecond to nanosecond backbone amide motions caused by the G121V mutation.

Side Chain Methyl ^{2}H Relaxation in the G121V E:FOL Complex. Methyl ^{2}H relaxation rates of $^{13}C^1H_2^2H$ methyl groups of the E:FOL complex were measured at ^{1}H spectrometer frequencies of 600 and 800 MHz. Methyl model-free parameters (S_{axis}^2 and τ_e) were determined by simultaneously fitting the ^{2}H quadrupolar relaxation at both magnetic fields (Figure 5) and were compared with parameters reported previously for the E:FOL complex of the WT enzyme (Figure 5B).[84] A complete set of calculated methyl model-free parameters is shown in Table S4 of the Supporting Information.

The changes in methyl S_{axis}^2 with the G121V mutation are consistent with the changes in backbone S^2 (Figures 3 and 4). Locations of changes in S_{axis}^2 between the mutant and WT are shown on the DHFR structure in Figure 6. Most notable are increases in S_{axis}^2 at Ala117-β in the FG loop and Ala19-β and Met20-ε in the Met20 loop in G121V DHFR. Smaller increases in S_{axis}^2 are observed for Val119-γ1/γ2 and Thr123-γ2 in the FG loop. Large increases in S_{axis}^2 also occur for Leu110-δ1/δ2 and Leu112-δ1/δ2 located in β-strand F at the center of the major subdomain β-sheet. These methyl groups are packed tightly against each other and against the aromatic ring of Phe125 in the C-terminal portion of the FG loop. The introduction of valine at site 121 provides two additional methyl probes in G121V. The Val121 methyls exhibit S_{axis}^2 values (0.26 and 0.28) significantly lower than the average for valine (0.71) but similar to that of Val119 (0.32 and 0.33), also in the central portion of the FG loop. Low values of S_{axis}^2 for Val119-γ1/γ2 and Val121-γ1/γ2 of G121V DHFR indicate that, although the amplitudes of motions are diminished relative to those of the WT, the FG loop remains flexible relative to the rest of the protein.

Backbone Microsecond to Millisecond Time Scale Dynamics of G121V Complexes. As the backbone microsecond to millisecond time scale dynamics of WT DHFR are very dependent on the nature of the bound ligands,[45,77] we used ^{15}N R_2 relaxation dispersion to study four complexes of G121V, including E:FOL, E:FOL:NADP$^+$, E:THF:NADP$^+$, and E:THF:NADPH. The WT E:FOL:NADP$^+$ complex has been previously used to model the reactive Michaelis complex (E:DHF:NADPH) of DHFR.[25,29,43] The E:FOL complex can

dx.doi.org/10.1021/bi400563c | Biochemistry 2013, 52, 4605−4619

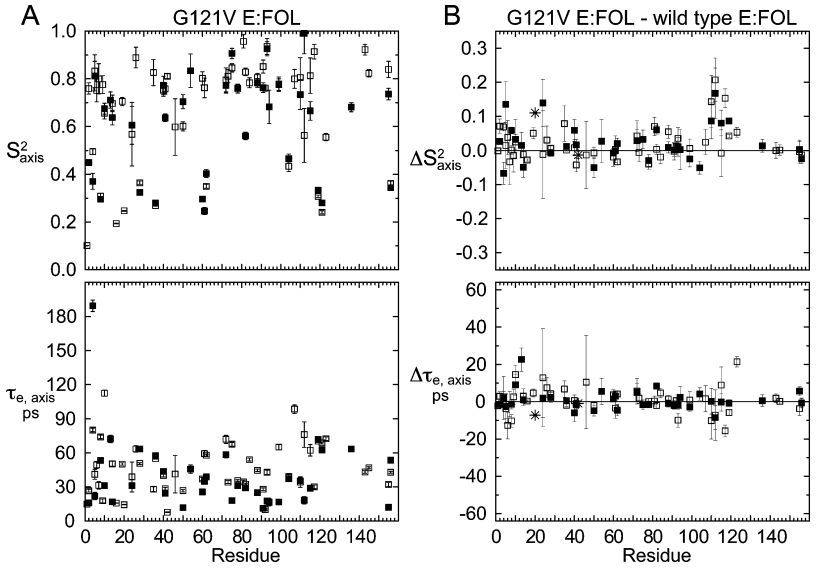

Figure 5. Model-free parameters derived from methyl-incorporated deuterium relaxation data for the E:FOL complex of G121V DHFR. Shown are the methyl axis order parameters (S_{axis}^2) and internal correlation times (τ_e) for (A) the G121V E:FOL complex and (B) the deviations from WT behavior. Differences are shown as G121V minus WT. Model-free parameters were extracted from fits to R_1 (^{2}H) and $R_{1\rho}$ (^{2}H) at ^{1}H spectrometer frequencies of 600 and 800 MHz. Model-free parameters for the WT complex are from ref 84. Parameters for Met20-ε and Met42-ε in WT DHFR were derived from 600 MHz (^{1}H frequency) spectra of a binary complex with dihydrofolate, used to resolve overlap in the spectra of the E:FOL complex.[84] Changes in dynamics for Met20 and Met42 are indicated with an asterisk in panel B: Ala-β, Thr-γ2, Met-ε, Ile-γ2, Leu-δ1, and Val-γ1 (□) and Ile-δ1, Leu-δ2, and Val-γ2 (■).

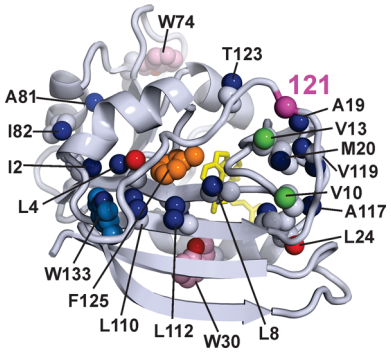

Figure 6. Location of methyl groups that show altered S_{axis}^2 values. Blue denotes increased motional restriction (decreased amplitude and increased S_{axis}^2), red an increased level of motion (decreased S_{axis}^2), and green methyl groups that show slower time scale motion (larger τ_e) in the G121V mutant. Tryptophan side chains that show changes in Nε order parameters or τ_e are shown. A red Nε or a pink side chain indicates increased flexibility, and a blue Nε or pale blue side chain indicates more restricted side chain dynamics in the mutant protein. The mutation site, Gly121, is indicated, and folate is shown as yellow sticks. Selected sites in the backbone and side chain are labeled. This figure was prepared using PyMOL.[99]

serve as a model for either the substrate binary (E:DHF) or product binary (E:THF) complex, although there are some notable changes in the WT backbone microsecond to millisecond time scale dynamics in the active-site loops between these complexes.[77] Altogether, these complexes represent four of the five major intermediates in the catalytic cycles of WT[24] and G121V DHFR.[34] The fifth complex, the holoenzyme (E:NADPH), is conformationally heterogeneous in the G121V complex, containing at least three different conformations,[29] and, as such, was not investigated further because of the complexity of its spectra. A summary of the data, including fits, for those residues exhibiting relaxation dispersion is shown in Figure S3 of the Supporting Information.

R_2 relaxation dispersion spectroscopy monitors conformational exchange events on the microsecond to millisecond time scale. For two-site exchange between states A and B, the magnitude of the exchange contribution to R_2 (R_{ex}) depends on the rate of exchange ($k_{ex} = k_{AB} + k_{BA}$), the populations of the states (p_A and p_B), and the chemical shift difference between them ($\Delta\omega$).[85] A major advantage of R_2 relaxation dispersion techniques is the ability to characterize minor populations comprising <5% of the conformational ensemble that is "invisible" to other structural techniques.[86]

^{15}N R_2 Relaxation Dispersion for the G121V E:FOL Complex. Residues in the WT and G121V E:FOL complexes that exhibit ^{15}N relaxation dispersion are shown in Figure 7A. For both the WT and mutant enzyme, conformational exchange is observed in the cofactor-binding cleft (green), the active-site loops (red), and the C-terminal associated region (blue). However, a major difference is observed in the folate-binding pocket (gold), where many residues exhibit conformational exchange processes in the G121V E:FOL complex but not in the WT complex (Figure 7A). For the WT enzyme, the dispersion data for residues in the active-site loops and cofactor-binding site can be fit to a single-exchange process for which $k_{ex} = k_{AB} + k_{BA} = 537$ s^{-1} and $p_B = 0.03$ at 306 K.[77] Similar kinetics are observed for residues in the active site and substrate binding site of the G121V mutant [$k_{ex} = 635$ s^{-1}, and $p_B = 0.017$ (Table 1)]. However, attempts to fit dispersion curves for residues in the active site, substrate binding site, and cofactor binding site with a global k_{ex} and p_B were unsatisfactory. Inclusion of the cofactor-site residues in the cluster fits resulted in a large decrease in k_{ex} and significantly worse fits (as indicated by χ^2) for many residues in the active-site loops and substrate binding site. We attempted unsuccessfully to fit the cofactor binding-site dispersion as a separate cluster; however, the data are of insufficient quality,

dx.doi.org/10.1021/bi400563c | Biochemistry 2013, 52, 4605−4619

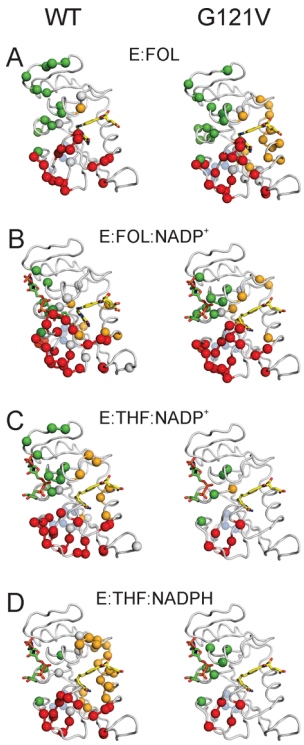

Figure 7. Comparison of microsecond to millisecond time scale backbone dynamics between WT (left) and G121V (right) DHFR complexes (A) E:FOL, (B) E:FOL:NADP$^+$, (C) E:THF:NADP$^+$, and (D) E:THF:NADPH. Residues displaying conformational exchange (R_{ex}) are highlighted as colored spheres [red for Met20, FG, and GH active-site loops, green for the cofactor-binding cleft, gold for the substrate/product binding site, gray for other residues, and pale blue (at the back of each structure) for the C-terminal associated region]. The coordinates used are from PDB entries 1RX7 (WT and G121V E:FOL) and 3QL3 and 1RX2 (WT E:FOL:NADP$^+$, a closed conformation). For everything else, the coordinate set from PDB entry 1RX6 [the 5,10-dideazatetrahydrofolate (ddTHF):NADPH complex] was used to model an occluded conformation with the adenosine ring bound but with the nicotinamide disordered and solvent-exposed outside the active site. Substrate molecules (ddTHF and FOL) are shown as yellow sticks, and cofactors (NADP$^+$ and NADPH) are shown as green and red (phosphate) sticks.

and residues 63, 65, and 77 in the adenosine-binding site appear to exhibit kinetics different from those of the other residues. Even though we were unable to obtain robust fits for these dispersion curves, our data suggest strongly that the G121V mutation has decoupled fluctuations in the cofactor site compared to those in the active site and has introduced new conformational fluctuations into the substrate binding pocket.

The relaxation dispersion observed for residues in the substrate binding site of the G121V E:FOL complex does not appear to reflect dissociation of folate. On the basis of the known dissociation constant, the free enzyme is estimated to have a population (0.01%) very much smaller than the population of the higher-energy substate ($p_B \sim 1\%$) determined using R_2 relaxation dispersion. As for the corresponding WT complex, the $\Delta\omega$ values for residues in the active-site loops of the G121V E:FOL complex differ from those expected for occluded−closed conformational transitions, indicating that the active-site fluctuations do not involve the formation of a closed excited state.

^{15}N R_2 Relaxation Dispersion for G121V Product Ternary Complexes. It is notable that, in comparison to the corresponding WT complexes, dispersion is relatively weak and limited to a small number of residues in both the E:THF:NADP$^+$ and E:THF:NADPH complexes of G121V. Conformational exchange is observed for the same residues in the Met20 loop and FG loop of both G121V complexes, suggesting that similar conformational transitions are involved (Figure 7C,D and Table S6 of the Supporting Information). As for the mutant E:FOL complex, the pattern of residues displaying dispersion and the dynamic chemical shift differences ($\Delta\omega$) indicate clearly that these fluctuations do not involve transitions to a closed excited state. It should be noted that Met20 loop residues with measurable conformational exchange also show small, but significant, chemical shift differences between the WT and G121V complexes (Figure 2). Weak dispersion is observed for several residues near the N-termini of helices αC and αF, at the site of binding of the pyrophosphate moiety of the cofactor, in both the E:THF:NADP$^+$ and E:THF:NADPH complexes of the G121V mutant. Conformational exchange is also observed in these regions in the WT E:THF:NADP$^+$ complex and extends into the adenosine-binding loop (Figure 7C).

The observed relaxation dispersion in the G121V E:THF:NADPH complex differs markedly from that in the corresponding complex of the WT enzyme[45] (Figure 7D). Conformational exchange in the mutant DHFR complex is limited to a small number of residues in the active-site loops, in the immediate proximity of the site of mutation, in the cofactor-binding site, and in the C-terminal associated region. In contrast, for the WT complex, conformational exchange occurs for many residues around the substrate/product binding site but not in the cofactor-binding cleft (Figure 7D). Thus, the microsecond to millisecond time scale dynamics in the product ternary complexes differ significantly for the WT and G121V mutant enzymes; the dynamics are very similar in the E:THF:NADP$^+$ and E:THF:NADPH complexes of the G121V mutant, whereas the corresponding complexes of the WT enzyme differ greatly in their microsecond to millisecond time scale motions.

^{15}N R_2 Relaxation Dispersion for the G121V E:FOL:NADP$^+$ Complex. Many more residues show dispersive behavior in the G121V E:FOL:NADP$^+$ complex than in the product ternary complexes of the mutant enzyme (Figure 7B). These include a large number of residues in the active-site loops, many of which also show dispersion in the WT E:FOL:NADP$^+$ complex (e.g., Asn18, Ala19, Met20, Trp22, Asn23, Gly96, Glu118, Val119, Glu120, Asp122, and His149) where they report on a "closed−occluded" conformational change.[43,87] However, for the G121V E:FOL:NADP$^+$ complex, there is no correlation between the dynamic chemical shifts ($\Delta\omega$) determined from R_2 relaxation dispersion and the equilibrium chemical shift difference ($\Delta\delta$) between closed and occluded conformations (Figure S4 of the Supporting Information), showing that the microsecond to millisecond time scale dynamics in the occluded active-site loops of the mutant complex do not lead to sampling of the closed state.

Although the Gibbs free energy differences between higher- and lower-energy substates are similar for the WT E:FOL:NADP$^+$, WT E:THF:NADP$^+$, and G121 V E:FOL:NADP$^+$ complexes, the enthalpy and entropy contributions differ significantly for the G121V E:FOL:NADP$^+$ complex (Table 2 and Figure 8). Again, this indicates that the higher-energy

Table 2. Comparison of Thermodynamic Parameters for WT and Gly121Val DHFR Microsecond to Millisecond Time Scale Dynamics at 300 K

thermodynamic parameter (kcal/mol)	WT E:FOL:NADP$^+$ closed → occluded[a]	WT E:THF:NADP$^+$ occluded → closed[a]	G121V E:FOL:NADP$^+$ occluded → ?
Energetic Differences between Higher-Energy and Ground-State Conformations			
ΔG	2.1 ± 0.3	2.7 ± 0.5	1.7 ± 0.0
ΔH	15.6 ± 2.1	13.9 ± 0.5	4.7 ± 0.4
$T\Delta S$	13.5 ± 2.1	11.2 ± 0.5	3.0 ± 0.4
Activation Energy Barrier Parameters			
$\Delta G^{\ddagger}$	16.0	15.9 ± 0.5	15.8 ± 0.1
$\Delta H^{\ddagger}$	21.2	20.3 ± 0.5	17.3 ± 1.9
$T\Delta S^{\ddagger}$	5.1	4.4 ± 0.5	1.5 ± 1.8

[a]Data for the WT complexes taken from ref 43 for E:FOL:NADP$^+$ and from the unpublished work of D. D. Boehr for E:THF:NADP$^+$.

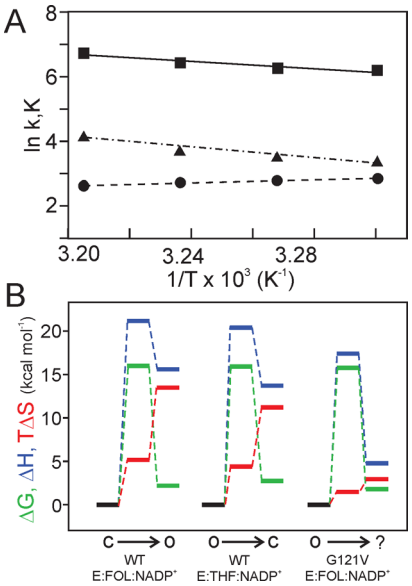

Figure 8. (A) Temperature dependence of the conformational exchange kinetics in the G121V E:FOL:NADP$^+$ complex for the active-site region. Rate constants for the transitions from the excited state to the ground state [k_{BA} (■)] and from the ground state to the excited state [k_{AB} (▲)] and the equilibrium constant [k_{BA}/k_{AB} (●)] are plotted. (B) Thermodynamic comparison of the G121V E:FOL:NADP$^+$ complex (occluded ground state, unknown excited state; o → ?) with the WT E:FOL:NADP$^+$ (closed ground state, occluded excited state; c → o) and WT E:THF:NADP$^+$ (occluded ground state, closed excited state; o → c) complexes at 298 K. Thermodynamic barriers were calculated using transition-state theory following Materials and Methods. ΔG, ΔH, and $T\Delta S$ traces are colored green, blue, and red, respectively.

conformation is not closed. It is interesting to note, however, that the energy barriers ($\Delta G^{\ddagger}$, $\Delta H^{\ddagger}$, and $T\Delta S^{\ddagger}$) associated with the microsecond to millisecond time scale dynamics are similar among all three complexes (Table 2 and Figure 8).

Microsecond to Millisecond Time Scale Dynamics in the C-Terminal Associated Region. All WT and G121V complexes show conformational exchange in the C-terminal associated region (residues 129−134 and 155−159). The C-terminal associated region appears to sample similar higher-energy conformational substates in all complexes, because $\Delta\omega$ values are similar for all WT and mutant enzyme complexes (Table S6 of the Supporting Information). However, it should be noted that the nature of the bound ligand(s) and the identity of the amino acid at position 121 influence the kinetics and thermodynamics of the fluctuations in this region (Tables 1 and 2). Neither the importance of the C-terminal dynamics nor the impact of ligand binding and/or mutagenesis on the motions in this region is understood.

DISCUSSION

E. coli DHFR has been widely used as a model system to investigate the relationship between protein dynamics and enzyme catalysis.[23] One key finding has been that mutations distant from the active-site center can significantly impact rates of hydride transfer.[26−28,35,88,89] This behavior is consistent with the suggestion that there is a catalytically important network of coupled protein motion extending from the enzyme surface into the active site.[9,19−21] A key residue in this network is Gly121, which resides in the FG loop and is more than 15 Å from the active-site center. To obtain further insights into the roles of Gly121 and protein motion in DHFR, we used NMR relaxation techniques to measure protein dynamics over the picosecond to millisecond time scales for complexes representing intermediates in the catalytic cycle of G121V DHFR.

Structural models indicate that the G121V substitution can be accommodated in the occluded state with only minor conformational adjustment. In contrast, incorporation of the bulky valine side chain would result in major steric clashes in the closed or open states that would necessitate substantial rearrangement of the Met20 and GH loop conformations and the packing interactions between them. Further, simulations suggest that substitution of valine at position 121 leads to Met20 loop conformations that differ substantially from the closed form and that a hydrogen bond between the Asp122 amide and Gly15 carbonyl, which helps stabilize the closed state, is disrupted.[90,91] The predicted destabilization of the closed state is supported by NMR data for the E:FOL:NADP$^+$ and E:FOL:NADPH complexes, which are in the fully closed conformation in the WT enzyme but adopt the occluded conformation in the corresponding complexes of the G121V mutant.[29] The G121V E:NADPH complex, which is closed for WT DHFR, is predominantly occluded but with a minor population of a closed state present in slow exchange;[29] addition of the inhibitor methotrexate (MTX) to form the E:NADPH:MTX ternary complex drives the G121V mutant into a fully closed state.[92]

Picosecond to Nanosecond Time Scale Dynamics in G121V DHFR. In the WT enzyme, picosecond to nanosecond time scale motions of DHFR are determined primarily by the overall backbone conformation (closed or occluded),[42,77] and we therefore used the E:FOL complex to probe picosecond to nanosecond time scale dynamics in the occluded conformations of G121V DHFR; all of the G121V complexes studied here, representing four of the intermediates of the catalytic cycle, are in the occluded conformation.

The picosecond to nanosecond time scale backbone and methyl side chain dynamics are overall quite similar for the WT and G121V E:FOL complexes, with the largest differences in S^2 and τ_e occurring at the site of mutation (Figures 3 and 4). The Val substitution decreases the amplitude (increased S^2) and changes the time scale (decreased τ_e) of the backbone motions of residues 120−123 in the FG loop (Figure 3). These changes in FG loop dynamics are transmitted to both local and distant sites in the protein.

dx.doi.org/10.1021/bi400563c | *Biochemistry* 2013, 52, 4605−4619

We first consider changes in side chain dynamics resulting from the incorporation of the bulky valine side chain. A decrease in the amplitude of side chain motions is observed for side chains in the FG loop that directly contact the side chain of Val121 (Val119 and Thr123). The motional changes are transmitted to the Ala19 and Met20 methyl groups in the Met20 loop, more than 8 Å from the site of mutation, as well as the Ala117 methyl and Ile115-δ1 methyl group at the beginning of the FG loop (Figure 6). The relaxation experiments thus reveal a general restriction of side chain motion in the Met20 and FG loops caused by the Val substitution and provide direct evidence of motional coupling between these regions of the protein. Our results are fully consistent with molecular dynamics simulations that revealed dynamic coupling between the Met20 and FG loops that is modulated by ligands and perturbed by the G121V substitution.[36,83] Importantly, however, the perturbations of DHFR dynamics extend far beyond the Met20 loop−FG loop interface to distant regions of the protein. Observed changes in methyl order parameters reveal a pathway by which dynamic perturbations can be communicated 25−30 Å across the protein molecule from the site of the G121V mutation (Figure 6). The motional changes propagate outward from the mutation site along the β-sheet, with restriction of the amplitude of side chain methyl groups of Leu8, Leu112, and Leu110 and of the Nε atom of Trp133. These residues are all in van der Waals contact and lie on one face of the β-sheet, packed against the aromatic ring of Phe125 that likely couples their motions to those of the FG loop. The side chain motional restrictions propagate further down strand βA to Leu4 and Ile2 and then into the adenosine-binding subdomain where increased order parameters are observed for Ile82 and Ala81 in helix αE and Val88 in the EF loop. There is also a substantial decrease in S^2 for the Nε atom of Trp74 in the CD loop, close to the adenosine-binding site. The changes in dynamics also extend, via Ile5 and Trp33, into the folate binding site.

The motional perturbations observed in the side chains are reflected in changes in picosecond to nanosecond time scale backbone dynamics. Although there is a decrease in the amplitude of backbone motions for residues 120−122 (average increase in S^2 of 0.14), the FG loop remains relatively flexible (Figure 3). Restriction of backbone dynamics is also observed for Asp11, Gly15, Glu17, and Asn18 in the Met20 loop, providing further evidence that the motions of the FG and Met20 loops are coupled.

The largest increase in backbone S^2 in the Met20 loop is seen for Glu17, which undergoes the largest structural changes between the occluded and closed conformations (the heavy atom rmsd between Glu17 in the occluded and closed loop conformations is 11.0 Å). The shortest distance between Glu17 and any FG loop residue in the crystallographically observed occluded conformation is >9 Å. However, given the high flexibility of the Met20 and FG loops, it seems likely that conformational sampling would bring these loops into transient contact. The importance of contacts between the FG and Met20 loops has been highlighted by mutational studies in which Asp122 is replaced by amino acids with side chains that are less able to hydrogen bond.[27]

The G121V mutation perturbs picosecond to nanosecond time scale backbone dynamics far beyond the Met20 loop, in regions of the protein that are more than 25 Å from the site of mutation. The extent of these perturbations is seen clearly in Figure 4B, which maps residues that show changes in the amplitude (S^2) and/or time scale (τ_e) of backbone motions onto the DHFR structure. It seems likely that these dynamic perturbations are propagated through the network of dynamically coupled side chains that lie on one face of the β-sheet at the core of the loop subdomain and are then transmitted to the adenosine-binding subdomain via contacts between the N-terminal region of strand βA and helix αE or are communicated via the bound folate ligand. For the majority of residues for which changes in picosecond to nanosecond dynamics are observed, the backbone motions become more restricted (larger S^2) in the G121V mutant. However, for a subset of residues at the C-terminal end of the FG loop, the C-terminus, and at Gln65 (also the nearby side chain of Trp74) in the adenosine-binding domain, the mutation increases the amplitude of the motions but shifts them to a slower time scale (Figure 4). Changes in backbone and side chain methyl group dynamics in the adenosine-binding domain arising from mutation of Gly121 to Val have also been reported for the complex of DHFR with NADPH and the drug methotrexate (MTX).[92] The NMR experiments thus provide insights into the molecular mechanism by which substitutions at Gly67 and Gly121 interact over long distances to exert nonadditive effects on the catalytic activity of DHFR.[33]

Mechanism of Allosteric Communication to Distant Sites. DHFR exhibits allosteric behavior in several ways. Binding of ligand in the substrate binding site alters the affinity for cofactor binding and vice versa.[24] Mutation of residues distant from the active site affects both binding affinity and hydride transfer kinetics, and nonadditive effects of double mutations provide evidence of coupled interaction networks spanning large distances within the protein.[33,35] The FG loop is connected to the active site via an evolutionarily conserved network of amino acids; insertion of a light sensitive LOV2 domain into DHFR between residues 120 and 121 results in weak light-dependent allosteric control of DHFR activity.[12,93]

These experiments show clearly that long-range structural changes are not a prerequisite for transmission of allosteric signals through a protein but that perturbations associated with a local event can be propagated by dynamic changes, i.e., by changes in the conformational space available for sampling through thermal fluctuations of the backbone or side chains. Figure 2A shows that the G121V mutation in the E:FOL complex leads to very few changes in backbone ^{1}H and ^{15}N chemical shifts, all of which are entirely localized to backbone amides lying within 9 Å of the site of mutation, in the FG loop itself, and in the tightly coupled Met20 loop (Figure 2A). The G121V mutant adopts an occluded conformation that is extremely close to that of the WT complex; however, the mutation leads to substantial changes in dynamics, restricting the amplitude and changing the time scale of motions of residues in the FG loop and in the neighboring Met20 loop. The effects of the mutation are transmitted to distant sites not through propagation of structural change, as evidenced by the almost complete absence of changes in chemical shifts for residues outside the site of mutation, but through subtle changes in the accessible conformational space sampled by molecular fluctuations on the picosecond to nanosecond time scale. Our results are fully consistent with theoretical approaches that suggest long-range allostery in DHFR arises from a redistribution of the conformational ensemble, with significant contributions from perturbations of the protein dynamics.[82]

Microsecond to Millisecond Time Scale Dynamics in G121V DHFR. In contrast to picosecond to nanosecond time scale dynamics of DHFR, the slower microsecond to millisecond time scale conformational fluctuations change significantly depending on the ligands that are bound to the enzyme.[45,77] It was therefore necessary to measure protein dynamics of several G121V complexes to elucidate the effect of mutation on these slower time scale dynamics.

The microsecond to millisecond time scale dynamics are quite similar for the FOL complexes of the WT and G121V protein, except in the substrate binding site (Figure 7A). Both exhibit extensive conformational fluctuations in the Met20 and FG loops, although the $\Delta\omega$ values for corresponding residues differ, suggesting that the WT and mutant proteins sample somewhat different conformational substates. Many residues in the cofactor binding site of the G121V E:FOL complex experience microsecond to millisecond time scale fluctuations, although the data presented here are of insufficient quality to quantitate this process. Fluctuations in the cofactor site were observed previously for WT E:THF[45] and E:FOL[77] complexes, and on the basis of chemical shift correlations, we have suggested[45] a conformational selection mechanism of ligand binding. There are two significant differences in dynamics between the WT and G121V E:FOL complexes: the microsecond to millisecond time scale fluctuations in the active-site loops propagate into the substrate binding site of the mutant enzyme but not WT, and the mutation appears to decouple the fluctuations in the cofactor binding site from the active-site motions, as was previously observed for the WT E:FOL:NADP$^+$ complex.[94] As for the picosecond to nanosecond time scale motions, the effects of the mutation are manifest in changes in microsecond to millisecond time scale dynamics in distant regions of the protein structure. Similar observations have been made for other enzymes; mutations in cyclophilin A and triosephosphate isomerase, for example, also result in perturbation of millisecond time scale fluctuations at distant sites.[95,96]

There are large differences in the microsecond to millisecond time scale dynamics between the product ternary complexes of the WT and G121V mutant enzyme. In the WT E:THF:NADP$^+$ complex, we observe four regions of conformational exchange: in the active-site loops, in the cofactor-binding cleft, for several residues in the proximity of the *p*-aminobenzoic acid moiety of the product THF, and in the C-terminal associated region.[94] These fluctuations are mostly impaired in the corresponding complex of the mutant, most notably in the product and cofactor binding sites (Figure 7C). In the WT E:THF:NADP$^+$ complex, there are widespread fluctuations in all three active-site loops (Met20, FG, and GH), reflecting conformational exchange between closed and occluded conformations of DHFR.[94] In contrast, very few residues in the Met20 and FG loops, all of which are in the immediate vicinity of the site of mutation, experience exchange in the G121V E:THF:NADP$^+$ complex. The $\Delta\omega$ values for these residues do not reflect transitions into a closed conformational state. Thus, the active-site region in the E:THF:NADP$^+$ complex of G121V fluctuates into an alternate conformational substate that differs from the closed state formed by the WT enzyme. In the C-terminal associated region, comparable microsecond to millisecond time scale dynamics are observed for WT and the G121V E:THF:NADP$^+$ complex, although there are small changes in the kinetics and thermodynamics (Table 1).

A very similar group of residues, located in the cofactor pyrophosphate binding site and in the immediate vicinity of the mutation site, exhibits microsecond to millisecond fluctuations in both the E:THF:NADPH and E:THF:NADP$^+$ complexes of the G121V enzyme (Figure 7C,D). Conformational exchange in the WT E:THF:NADPH complex is far more widespread than in the G121V mutant, with many residues in the Met20, FG, and GH loops exhibiting relaxation dispersion[45] (Figure 7D). Most importantly, numerous residues in the THF binding site undergo conformational fluctuations in the WT E:THF:NADPH complex that are completely abrogated in the G121V mutant. We have previously proposed that conformational fluctuations in the substrate/product binding pocket of the WT E:THF:NADPH complex play a key role in the release of product, because the rate of lower- to higher-energy substate conversion (k_{AB} = 12−18 s^{-1}) is very similar to the THF dissociation rate constant (k_{off} = 13 s^{-1}).[45] The loss of these fluctuations in the G121V E:THF:NADPH complex is consistent with the decreased dissociation rate constant for THF for the mutant enzyme (k_{off} = 1.9 s^{-1}),[34] which is too slow to give measurable R_2 relaxation dispersion. Instead, for the G121V E:THF:NADPH complex, we observe microsecond to millisecond time scale dynamics in helix αC, which forms the binding site for the ribose phosphate region of the cofactor. The structural fluctuations in the cofactor-binding cleft of the G121V E:THF:NADPH complex, which we cannot detect in the corresponding WT complex using R_2 relaxation dispersion,[45] may also explain why the dissociation rate constant of NADPH is 3 times higher in the G121V protein than in the WT enzyme.[34]

As noted above, the microsecond to millisecond time scale dynamics of the product ternary complexes (E:THF:NADP$^+$ and E:THF:NADPH) are similar for the G121V mutant but differ for the WT enzyme. We have shown elsewhere[45,77] that the conformational fluctuations in the active-site loops for the ternary product complexes of the WT enzyme allow the nicotinamide ring to transiently enter the active-site pocket. The different charge and/or shape of the reduced and oxidized forms of the ring leads to different dynamic behavior in the substrate and cofactor binding pockets for the E:THF:NADPH and E:THF:NADP$^+$ complexes of the WT protein.[45,77] Because we cannot detect similar active-site loop motions in the G121V complexes, it appears that, on the time scale of R_2 relaxation dispersion, the nicotinamide ring cannot transiently enter the active site to affect dynamics in the substrate and cofactor binding sites. These findings suggest that the G121V mutation has uncoupled the active-site loop motions and the concomitant motion of the nicotinamide ring into the active site from structural fluctuations in the binding pockets for the cofactor and substrate/product. Structural fluctuations in the substrate/product binding pocket still depend on the motions of the active-site loops and the nicotinamide ring, whereas those in the cofactor binding site are now independent.

Perhaps the most relevant complex for elucidating the role of Gly121 in DHFR-catalyzed hydride transfer is the G121V E:FOL:NADP$^+$ complex. It has been suggested that the E:FOL:NADP$^+$ complex serves as a good model for the reactive E:DHF:NADPH (Michaelis) complex.[25,29,43] The E:FOL:NADP$^+$ complex of the WT enzyme adopts a closed ground-state conformation that allows for close association between the pterin and nicotinamide rings. However, the G121V E:FOL:NADP$^+$ complex is clearly not in the closed conformation. Moreover, there is no experimental evidence

dx.doi.org/10.1021/bi400563c | *Biochemistry* 2013, 52, 4605−4619

from the R_2 relaxation dispersion experiments that the G121V complex even samples the closed conformation in thermally accessible higher-energy states. Our results suggest that if the G121V E:FOL:NADP$^+$ complex does fluctuate from its occluded ground state into a closed conformation, either the kinetics of conformational exchange are too slow (i.e., $k_{ex} < 100$ s^{-1}) or the population of the closed conformation is too small (i.e., $p_B < 1\%$) to observe by R_2 relaxation dispersion. It should be noted that pre-steady-state kinetic analysis of the G121V enzyme revealed an additional step, not observed for the WT enzyme, associated with a conformational change that precedes hydride transfer.[34] This process, with a rate constant of 3.5 s^{-1} (at 298 K), is too slow to be detected by R_2 relaxation dispersion. Thus, there are potentially two conformational changes in the G121V E:FOL:NADP$^+$ complex. The first conformational change involving several of the Met20, FG, and GH loop residues, which we can detect using R_2 relaxation dispersion ($k \sim 25$ s^{-1} at 303 K), may poise the enzyme for the second conformational change ($k \sim 3.5$ s^{-1}) to the closed, catalytically competent state, with the nicotinamide ring bound in the active site. Although all of the intermediates from the catalytic cycle adopt the fully occluded conformation, G121V can be forced into the closed state by binding NADPH and the drug methotrexate.[92] Conformational fluctuations are observed in the Met20 and FG loops of the G121V E:NADPH:MTX complex, but amide resonances are severely exchange broadened, precluding identification of the structure of the state involved in the exchange.

Our results clearly indicate that conformational sampling is different between WT and G121V DHFR and provide insights into the molecular basis for the changes in both ligand affinities and the hydride transfer rate. It is noteworthy that many of the residues identified as being part of the network of coupled promoting motions have different picosecond to nanosecond and/or microsecond to millisecond time scale dynamics in the G121V and WT complexes, including residues Ile14, Gly15, Tyr100, and Asp122.[9] The side chains of several aliphatic residues in and around the active site become more rigid in G121V, and this may also impair the coupled motional network that promotes catalysis. Overall, the changes in the dynamics of the enzyme upon mutation of Gly121 to Val provide compelling evidence of motional coupling between residue 121 and other residues in the network.

Our findings are also entirely consistent with the dynamic energy landscape view of enzyme catalysis.[45] Changes in the kinetics and thermodynamics of conformational exchange and/or the nature of the higher-energy substates can lead to substantial changes in enzyme function. For the E:THF:NADPH complex, the lowest-energy conformation is very similar for the WT and G121V enzymes, and thus, differences in ligand dissociation appear to depend on differences in conformational sampling. In the case of the model Michaelis E:FOL:NADP$^+$ complex, the nature of both the ground state and higher-energy substates can help explain the 200-fold reduction in the hydride transfer rate of the G121V enzyme compared to that of the WT protein. Thus, both the ground state and higher-energy conformations of DHFR participate in enzyme catalysis. Our studies demonstrate that functional changes upon mutation not only are dependent on structural changes in the lowest-energy conformations but also can be propagated through changes in the higher-energy conformations and/or overall protein dynamics. This suggests novel forms of dynamic allostery[7,14−18] and offers new dimensions for molecular evolution.[97,98]

■ ASSOCIATED CONTENT

Supporting Information

Tables showing excluded residues, model-free diffusion parameters, methyl order parameters, kinetic and thermodynamic parameters, and dynamic chemical shift differences and plots of ^{15}N relaxation parameters, diffusion coefficients, and relaxation dispersion curves. This material is available free of charge via the Internet at http://pubs.acs.org.

■ AUTHOR INFORMATION

Corresponding Author

*Department of Integrative Structural and Computational Biology, The Scripps Research Institute, 10550 N. Torrey Pines Rd., La Jolla, CA 92037. E-mail: wright@scripps.edu. Phone: (858) 784-9721.

Present Addresses

[§]D.D.B.: Department of Chemistry, The Pennsylvania State University, University Park, PA 16802.

[∥]J.R.S.: Department of Biochemistry, University of Oxford, South Parks Road, Oxford OX1 3QU, U.K.

[⊥]D.M.: Department of Chemistry, University of Illinois at Chicago, 845 W. Taylor St., MC 111, Chicago, IL 60607.

[@]S.-H.B.: Nymirum, 3510 W. Liberty Rd., Ann Arbor, MI 48103.

[#]B.M.D.: UC San Diego Skaggs School of Pharmacy and Pharmaceutical Sciences, 9500 Gilman Dr., La Jolla, CA 92093.

Author Contributions

D.D.B., J.R.S., and D.M. contributed equally to this work.

Funding

This work was supported by Grant GM75995 from the National Institutes of Health and by the Skaggs Institute for Chemical Biology. D.D.B. acknowledges support from a Canadian Institutes of Health Research (CIHR) postdoctoral fellowship.

Notes

The authors declare no competing financial interest.

■ ACKNOWLEDGMENTS

We thank Linda Tennant and Euvel Manlapaz for technical support and John Chung and Gerard Kroon for their help with the NMR experiments.

■ ABBREVIATIONS

DHFR, dihydrofolate reductase; NMR, nuclear magnetic resonance; NADP$^+$, nicotinamide adenine dinucleotide phosphate; NADPH, reduced nicotinamide adenine dinucleotide phosphate; DHF, 7,8-dihydrofolate; THF, 5,6,7,8-tetrahydrofolate; MTX, methotrexate; CSA, chemical shift anisotropy; NOE, nuclear Overhauser effect; COPED, comparison of predicted and experimental diffusion tensors; rmsd, root-mean-square deviation; PDB, Protein Data Bank.

■ REFERENCES

(1) Zhou, H. X., Wlodek, S. T., and McCammon, J. A. (1998) Conformation gating as a mechanism for enzyme specificity. *Proc. Natl. Acad. Sci. U.S.A. 95*, 9280−9283.

(2) Antoniou, D., Caratzoulas, S., Kalyanaraman, C., Mincer, J. S., and Schwartz, S. D. (2002) Barrier passage and protein dynamics in enzymatically catalyzed reactions. *Eur. J. Biochem. 269*, 3103−3112.

(3) Benkovic, S. J., and Hammes-Schiffer, S. (2003) A perspective on enzyme catalysis. *Science 301*, 1196−1202.
(4) Tousignant, A., and Pelletier, J. N. (2004) Protein motions promote catalysis. *Chem. Biol. 11*, 1037−1042.
(5) Liang, Z. X., and Klinman, J. P. (2004) Structural bases of hydrogen tunneling in enzymes: Progress and puzzles. *Curr. Opin. Struct. Biol. 14*, 648−655.
(6) Boehr, D. D., Dyson, H. J., and Wright, P. E. (2006) An NMR perspective on enzyme dynamics. *Chem. Rev. 106*, 3055−3079.
(7) Goodey, N. M., and Benkovic, S. J. (2008) Allosteric regulation and catalysis emerge via a common route. *Nat. Chem. Biol. 4*, 474−482.
(8) Benkovic, S. J., Hammes, G. G., and Hammes-Schiffer, S. (2008) Free-Energy Landscape of Enzyme Catalysis. *Biochemistry 47*, 3317−3321.
(9) Agarwal, P. K., Billeter, S. R., Rajagopalan, P. T. R., Benkovic, S. J., and Hammes-Schiffer, S. (2002) Network of coupled promoting motions in enzyme catalysis. *Proc. Natl. Acad. Sci. U.S.A. 99*, 2794−2799.
(10) Tanikawa, J., Nomura, T., Macmillan, E. M., Shinagawa, T., Jin, W., Kokura, K., Baba, D., Shirakawa, M., Gonda, T. J., and Ishii, S. (2004) p53 suppresses c-Myb-induced trans-activation and trans-formation by recruiting the corepressor mSin3A. *J. Biol. Chem. 279*, 55393−55400.
(11) Lockless, S. W., and Ranganathan, R. (1999) Evolutionarily conserved pathways of energetic connectivity in protein families. *Science 286*, 295−299.
(12) Reynolds, K. A., McLaughlin, R. N., and Ranganathan, R. (2011) Hot Spots for Allosteric Regulation on Protein Surfaces. *Cell 147*, 1564−1575.
(13) Dhulesia, A., Gsponer, J., and Vendruscolo, M. (2008) Mapping of Two Networks of Residues That Exhibit Structural and Dynamical Changes upon Binding in a PDZ Domain Protein. *J. Am. Chem. Soc. 130*, 8931−8939.
(14) Cooper, A., and Dryden, D. T. (1984) Allostery without conformational change. A plausible model. *Eur. Biophys. J. 11*, 103−109.
(15) Kern, D., and Zuiderweg, E. R. (2003) The role of dynamics in allosteric regulation. *Curr. Opin. Struct. Biol. 13*, 748−757.
(16) Popovych, N., Sun, S., Ebright, R. H., and Kalodimos, C. G. (2006) Dynamically driven protein allostery. *Nat. Struct. Mol. Biol. 13*, 831−838.
(17) Swain, J. F., and Gierasch, L. M. (2006) The changing landscape of protein allostery. *Curr. Opin. Struct. Biol. 16*, 102−108.
(18) Tsai, C. J., del Sol, A., and Nussinov, R. (2008) Allostery: Absence of a change in shape does not imply that allostery is not at play. *J. Mol. Biol. 378*, 1−11.
(19) Sergi, A., Watney, J. B., Wong, K. F., and Hammes-Schiffer, S. (2006) Freezing a single distal motion in dihydrofolate reductase. *J. Phys. Chem. B 110*, 2435−2441.
(20) Watney, J. B., Agarwal, P. K., and Hammes-Schiffer, S. (2003) Effect of mutation on enzyme motion in dihydrofolate reductase. *J. Am. Chem. Soc. 125*, 3745−3750.
(21) Wong, K. F., Selzer, T., Benkovic, S. J., and Hammes-Schiffer, S. (2005) Impact of distal mutations on the network of coupled motions correlated to hydride transfer in dihydrofolate reductase. *Proc. Natl. Acad. Sci. U.S.A. 102*, 6807−6812.
(22) Chen, J., Dima, R. I., and Thirumalai, D. (2007) Allosteric Communication in Dihydrofolate Reductase: Signaling Network and Pathways for Closed to Occluded Transition and Back. *J. Mol. Biol. 374*, 250−266.
(23) Schnell, J. R., Dyson, H. J., and Wright, P. E. (2004) Structure, dynamics and catalytic function of dihydrofolate reductase. *Annu. Rev. Biophys. Biomol. Struct. 33*, 119−140.
(24) Fierke, C. A., Johnson, K. A., and Benkovic, S. J. (1987) Construction and evaluation of the kinetic scheme associated with dihydrofolate reductase from *Escherichia coli*. *Biochemistry 26*, 4085−4092.
(25) Sawaya, M. R., and Kraut, J. (1997) Loop and subdomain movements in the mechanism of *Escherichia coli* dihydrofolate reductase: Crystallographic evidence. *Biochemistry 36*, 586−603.
(26) Miller, G. P., and Benkovic, S. J. (1998) Deletion of a highly motional residue affects formation of the Michaelis complex for *Escherichia coli* dihydrofolate reductase. *Biochemistry 37*, 6327−6335.
(27) Miller, G. P., and Benkovic, S. J. (1998) Strength of an interloop hydrogen bond determines the kinetic pathway in catalysis by *Escherichia coli* dihydrofolate reductase. *Biochemistry 37*, 6336−6342.
(28) Miller, G. P., Wahnon, D. C., and Benkovic, S. J. (2001) Interloop contacts modulate ligand cycling during catalysis by *Escherichia coli* dihydrofolate reductase. *Biochemistry 40*, 867−875.
(29) Venkitakrishnan, R. P., Zaborowski, E., McElheny, D., Benkovic, S. J., Dyson, H. J., and Wright, P. E. (2004) Conformational changes in the active site loops of dihydrofolate reductase during the catalytic cycle. *Biochemistry 43*, 16046−16055.
(30) Antikainen, N. M., Smiley, R. D., Benkovic, S. J., and Hammes, G. G. (2005) Conformation coupled enzyme catalysis: Single-molecule and transient kinetics investigation of dihydrofolate reductase. *Biochemistry 44*, 16835−16843.
(31) Gekko, K., Kunori, Y., Takeuchi, H., Ichihara, S., and Kodama, M. (1994) Point mutations at glycine-121 of *Escherichia coli* dihydrofolate reductase: Important roles of a flexible loop in the stability and function. *J. Biochem. 116*, 34−41.
(32) Gekko, K., Yamagami, K., Kunori, Y., Ichibara, S., Kodama, M., and Iwakura, M. (1993) Effects of point mutation in a flexible loop on the stability and enzymatic function of *Escherichia coli* dihydrofolate reductase. *J. Biochem. 113*, 74−80.
(33) Ohmae, E., Iriyama, K., Ichihara, S., and Gekko, K. (1998) Nonadditive effects of double mutations at the flexible loops, glycine-67 and glycine-121, of *Escherichia coli* dihydrofolate reductase on its stability and function. *J. Biochem. 123*, 33−41.
(34) Cameron, C. E., and Benkovic, S. J. (1997) Evidence for a functional role of the dynamics of glycine-121 of *Escherichia coli* dihydrofolate reductase obtained from kinetic analysis of a site-directed mutant. *Biochemistry 36*, 15792−15800.
(35) Rajagopalan, P. T., Lutz, S., and Benkovic, S. J. (2002) Coupling interactions of distal residues enhance dihydrofolate reductase catalysis: Mutational effects on hydride transfer rates. *Biochemistry 41*, 12618−12628.
(36) Rod, T. H., Radkiewicz, J. L., and Brooks, C. L. (2003) Correlated motion and the effect of distal mutations in dihydrofolate reductase. *Proc. Natl. Acad. Sci. U.S.A. 100*, 6980−6985.
(37) Sikorski, R. S., Wang, L., Markham, K. A., Rajagopalan, P. T., Benkovic, S. J., and Kohen, A. (2004) Tunneling and coupled motion in *Escherichia coli* dihydrofolate reductase catalysis. *J. Am. Chem. Soc. 126*, 4778−4779.
(38) Wang, L., Tharp, S., Selzer, T., Benkovic, S. J., and Kohen, A. (2006) Effects of a distal mutation on active site chemistry. *Biochemistry 45*, 1383−1392.
(39) Wang, L., Goodey, N. M., Benkovic, S. J., and Kohen, A. (2006) The role of enzyme dynamics and tunnelling in catalysing hydride transfer: Studies of distal mutants of dihydrofolate reductase. *Philos. Trans. R. Soc., B 361*, 1307−1315.
(40) Epstein, D. M., Benkovic, S. J., and Wright, P. E. (1995) Dynamics of the dihydrofolate reductase folate complex: Catalytic sites and regions known to undergo conformational change exhibit diverse dynamical features. *Biochemistry 34*, 11037−11048.
(41) Falzone, C. J., Wright, P. E., and Benkovic, S. J. (1994) Dynamics of a flexible loop in dihydrofolate reductase from *Escherichia coli* and its implication for catalysis. *Biochemistry 33*, 439−442.
(42) Osborne, M. J., Schnell, J., Benkovic, S. J., Dyson, H. J., and Wright, P. E. (2001) Backbone dynamics in dihydrofolate reductase complexes: Role of loop flexibility in the catalytic mechanism. *Biochemistry 40*, 9846−9859.
(43) McElheny, D., Schnell, J. R., Lansing, J. C., Dyson, H. J., and Wright, P. E. (2005) Defining the role of active-site loop fluctuations in dihydrofolate reductase catalysis. *Proc. Natl. Acad. Sci. U.S.A. 102*, 5032−5037.

(44) Swinger, K. K., and Rice, P. A. (2007) Structure-based Analysis of HU-DNA Binding. *J. Mol. Biol. 365*, 1005−1016.
(45) Boehr, D. D., McElheny, D., Dyson, H. J., and Wright, P. E. (2006) The dynamic energy landscape of dihydrofolate reductase catalysis. *Science 313*, 1638−1642.
(46) Swint-Kruse, L., and Fisher, H. F. (2008) Enzymatic reaction sequences as coupled multiple traces on a multidimensional landscape. *Trends Biochem. Sci. 33*, 104−112.
(47) Grzesiek, S., and Bax, A. (1992) Correlating backbone amide and side chain resonances in larger proteins by multiple relayed triple resonance NMR. *J. Am. Chem. Soc. 114*, 6291−6293.
(48) Wittekind, M., and Mueller, L. (1993) HNCACB, a high-sensitivity 3D NMR experiment to correlate amide-proton and nitrogen resonances with the α- and β-carbon resonances in proteins. *J. Magn. Reson. 101*, 201−205.
(49) Muhandiram, D. R., and Kay, L. E. (1994) Gradient-enhanced triple-resonance three-dimensional NMR experiments with improved sensitivity. *J. Magn. Reson., Ser. B 103*, 203−216.
(50) Yamazaki, T., Lee, W., Revington, M., Mattiello, D. L., Dahlquist, F. W., Arrowsmith, C. H., and Kay, L. E. (1994) An HNCA pulse scheme for the backbone assignment of ^{15}N, ^{13}C, ^{2}H-labeled Proteins: Application to a 37-kDa *Trp* repressor-DNA complex. *J. Am. Chem. Soc. 116*, 6464−6465.
(51) Kay, L. E., Ikura, M., and Bax, A. (1990) Proton-proton correlation via carbon-carbon couplings: A three-dimensional NMR approach for the assignment of aliphatic resonances in proteins labeled with carbon-13. *J. Am. Chem. Soc. 112*, 888−889.
(52) Montelione, G. T., Lyons, B. A., Emerson, S. D., and Tashiro, M. (1992) An efficient triple resonance experiment using carbon-13 isotropic mixing for determining sequence-specific resonance assignments of isotopically-enriched proteins. *J. Am. Chem. Soc. 114*, 10974−10975.
(53) Farrow, N. A., Zhang, O., Forman-Kay, J. D., and Kay, L. E. (1995) Comparison of the backbone dynamics of a folded and an unfolded SH3 domain existing in solution in aqueous buffer. *Biochemistry 34*, 868−878.
(54) Jones, J. A., Hodgkinson, P., Barker, A. L., and Hore, P. J. (1996) Optimal sampling strategies for the measurement of spin-spin relaxation times. *J. Magn. Reson. 113*, 25−34.
(55) Palmer, A. G., Cavanagh, J., Wright, P. E., and Rance, M. (1991) Sensitivity improvement in proton-detected two-dimensional heteronuclear correlation NMR spectroscopy. *J. Magn. Reson. 93*, 151−170.
(56) Press, W. H., Teukolsky, S. A., Vetterling, W. T., and Flannery, B. P. (1992) *Numerical Recipes in C*, Cambridge University Press, Cambridge U.K.
(57) Markley, J. L., Horseley, W. J., and Klein, M. P. (1971) Spin-lattice relaxation in slowly relaxing complex spectra. *J. Chem. Phys. 55*, 3604−3605.
(58) Schurr, J. M., Babcock, H. P., and Fujimoto, B. S. (1994) A test of the model-free formulas. Effects of anisotropic rotational diffusion and dimerization. *J. Magn. Reson., Ser. B 105*, 211−224.
(59) Osborne, M. J., and Wright, P. E. (2001) Anisotropic rotational diffusion in model-free analysis for a ternary-DHFR complex. *J. Biomol. NMR 19*, 209−230.
(60) Korzhnev, D. M., Orekhov, V. Y., and Arseniev, A. S. (1997) Model-free approach beyond the borders of its applicability. *J. Magn. Reson. 127*, 184−191.
(61) Garcia de la Torre, J. G., and Bloomfield, V. A. (1981) Hydrodynamic properties of complex, rigid, biological macromolecules: Theory and applications. *Q. Rev. Biophys. 14*, 81−139.
(62) Lee, L. K., Rance, M., Chazin, W. J., and Palmer, A. G. (1997) Rotational diffusion anisotropy of proteins from simultaneous analysis of ^{15}N and ^{13}C alpha nuclear spin relaxation. *J. Biomol. NMR 9*, 287−298.
(63) Kroenke, C. D., Rance, M., and Palmer, A. G. (1999) Variability of the ^{15}N chemical shift anisotropy in *Escherichia coli* ribonuclease H in solution. *J. Am. Chem. Soc. 121*, 10119−10125.
(64) Case, D. A. (1999) Calculations of NMR dipolar coupling strengths in model peptides. *J. Biomol. NMR 15*, 95−102.
(65) Clore, G. M., Szabo, A., Bax, A., Kay, L. E., Driscoll, P. C., and Gronenborn, A. M. (1990) Deviations from the simple two-parameter model-free approach to the interpretation of nitrogen-15 nuclear magnetic relaxation of proteins. *J. Am. Chem. Soc. 112*, 4989−4991.
(66) d'Auvergne, E. J., and Gooley, P. R. (2003) The use of model selection in the model-free analysis of protein dynamics. *J. Biomol. NMR 25*, 25−39.
(67) Chen, J., Brooks, C. L., and Wright, P. E. (2004) Model-free analysis of protein dynamics: Assessment of accuracy and model selection protocols based on molecular dynamics simulations. *J. Biomol. NMR 29*, 243−257.
(68) Ebert, M. O., Bae, S. H., Dyson, H. J., and Wright, P. E. (2008) NMR relaxation study of the complex formed between CBP and the activation domain of the nuclear hormone receptor coactivator ACTR. *Biochemistry 47*, 1299−1308.
(69) Muhandiram, D. R., Yamazaki, T., Sykes, B. D., and Kay, L. E. (1995) Measurement of ^{2}H T_1 and $T_{1\rho}$ relaxation times in uniformly ^{13}C-labeled and fractionally ^{2}H-labeled proteins in solution. *J. Am. Chem. Soc. 117*, 11536−11544.
(70) Palmer, A. G., Rance, M., and Wright, P. E. (1991) Intramolecular motions of a zinc finger DNA-binding domain from Xfin characterized by proton-detected natural abundance ^{13}C NMR spectroscopy. *J. Am. Chem. Soc. 113*, 4371−4380.
(71) Viles, J. H., Duggan, B. M., Zaborowski, E., Schwarzinger, S., Huntley, J. J., Kroon, G. J., Dyson, H. J., and Wright, P. E. (2001) Potential bias in NMR relaxation data introduced by peak intensity analysis and curve fitting methods. *J. Biomol. NMR 21*, 1−9.
(72) Abragam, A. (1961) *Principles of Nuclear Magnetism*, Clarendon Press, Oxford, U.K.
(73) Mittermaier, A., Kay, L. E., and Forman-Kay, J. D. (1999) Analysis of deuterium relaxation-derived methyl axis order parameters and correlation with local structure. *J. Biomol. NMR 13*, 181−185.
(74) Kay, L. E., Torchia, D. A., and Bax, A. (1989) Backbone dynamics of proteins as studied by ^{15}N inverse detected heteronuclear NMR spectroscopy: Application to staphylococcal nuclease. *Biochemistry 28*, 8972−8979.
(75) Loria, J. P., Rance, M., and Palmer, A. G. (1999) A relaxation-compensated Carr-Purcell-Meiboom-Gill sequence for characterizing chemical exchange by NMR spectroscopy. *J. Am. Chem. Soc. 121*, 2331−2332.
(76) Skrynnikov, N. R., Dahlquist, F. W., and Kay, L. E. (2002) Reconstructing NMR spectra of "invisible" excited protein states using HSQC and HMQC experiments. *J. Am. Chem. Soc. 124*, 12352−12360.
(77) Boehr, D. D., McElheny, D., Dyson, H. J., and Wright, P. E. (2010) Millisecond timescale fluctuations in dihydrofolate reductase are exquisitely sensitive to the bound ligands. *Proc. Natl. Acad. Sci. U.S.A. 107*, 1373−1378.
(78) Ferrage, F., Cowburn, D., and Ghose, R. (2009) Accurate sampling of high-frequency motions in proteins by steady-state ^{15}N-{^{1}H} nuclear Overhauser effect measurements in the presence of cross-correlated relaxation. *J. Am. Chem. Soc. 131*, 6048−6049.
(79) Lipari, G., and Szabo, A. (1982) Model-free approach to the interpretation of nuclear magnetic resonance relaxation in macromolecules. 2. Analysis of experimental results. *J. Am. Chem. Soc. 104*, 4559−4570.
(80) Lipari, G., and Szabo, A. (1982) Model-free approach to the interpretation of nuclear magnetic resonance relaxation in macromolecules. 1. Theory and range of validity. *J. Am. Chem. Soc. 104*, 4546−4559.
(81) Ohmae, E., Iriyama, K., Ichihara, S., and Gekko, K. (1996) Effects of point mutations at the flexible loop glycine-67 of *Escherichia coli* dihydrofolate reductase on its stability and function. *J. Biochem. 119*, 703−710.
(82) Pan, H., Lee, J. C., and Hilser, V. J. (2000) Binding sites in *Escherichia coli* dihydrofolate reductase communicate by modulating the conformational ensemble. *Proc. Natl. Acad. Sci. U.S.A. 97*, 12020−12025.

(83) Radkiewicz, J. L., and Brooks, C. L. (2000) Protein dynamics in enzymatic catalysis: Exploration of dihydrofolate reductase. *J. Am. Chem. Soc. 122*, 225−231.
(84) Schnell, J. R., Dyson, H. J., and Wright, P. E. (2004) Effect of cofactor binding and loop conformation on side chain methyl dynamics in dihydrofolate reductase. *Biochemistry 43*, 374−383.
(85) Palmer, A. G. (2001) NMR probes of molecular dynamics: Overview and comparison with other techniques. *Annu. Rev. Biophys. Biomol. Struct. 30*, 129−155.
(86) Mittermaier, A., and Kay, L. E. (2006) New Tools Provide New Insights in NMR Studies of Protein Dynamics. *Science 312*, 224−228.
(87) Osborne, M. J., Venkitakrishnan, R. P., Dyson, H. J., and Wright, P. E. (2003) Diagnostic chemical shift markers for loop conformation and cofactor binding in dihydrofolate reductase complexes. *Protein Sci. 12*, 2230−2238.
(88) Adams, J., Johnson, K., Matthews, R., and Benkovic, S. J. (1989) Effects of distal point-site mutations on the binding and catalysis of dihydrofolate reductase from *Escherichia coli*. *Biochemistry 28*, 6611−6618.
(89) Wagner, C. R., Huang, Z., Singleton, S. F., and Benkovic, S. J. (1995) Molecular basis for nonadditive mutational effects in *Escherichia coli* dihydrofolate reductase. *Biochemistry 34*, 15671−15680.
(90) Thorpe, I. F., and Brooks, C. L. (2003) Barriers to hydride transfer in wild type and mutant dihydrofolate reductase from *E. coli*. *J. Phys. Chem. B 107*, 14042−14051.
(91) Thorpe, I. F., and Brooks, C. L. (2004) The coupling of structural fluctuations to hydride transfer in dihydrofolate reductase. *Proteins 57*, 444−457.
(92) Mauldin, R. V., Sapienza, P. J., Petit, C. M., and Lee, A. L. (2012) Structure and dynamics of the G121V dihydrofolate reductase mutant: Lessons from a transition-state inhibitor complex. *PLoS One 7*, e33252.
(93) Lee, J., Natarajan, M., Nashine, V. C., Socolich, M., Vo, T., Russ, W. P., Benkovic, S. J., and Ranganathan, R. (2008) Surface sites for engineering allosteric control in proteins. *Science 322*, 438−442.
(94) Boehr, D. D., Dyson, H. J., and Wright, P. E. (2008) Conformational relaxation following hydride transfer plays a limiting role in dihydrofolate reductase catalysis. *Biochemistry 47*, 9227−9233.
(95) Eisenmesser, E. Z., Millet, O., Labeikovsky, W., Korzhnev, D. M., Wolf-Watz, M., Bosco, D. A., Skalicky, J. J., Kay, L. E., and Kern, D. (2005) Intrinsic dynamics of an enzyme underlies catalysis. *Nature 438*, 117−121.
(96) Wang, Y., Berlow, R. B., and Loria, J. P. (2009) Role of loop-loop interactions in coordinating motions and enzymatic function in triosephosphate isomerase. *Biochemistry 48*, 4548−4556.
(97) Ma, B. Y., Wolfson, H. J., and Nussinov, R. (2001) Protein functional epitopes: Hot spots, dynamics and combinatorial libraries. *Curr. Opin. Struct. Biol. 11*, 364−369.
(98) James, L. C., and Tawfik, D. S. (2003) Conformational diversity and protein evolution: A 60-year-old hypothesis revisited. *Trends Biochem. Sci. 28*, 361−368.
(99) *The PyMOL Molecular Graphics System* (2013) Schrödinger, LLC.
(100) Otting, G. (1993) Experimental NMR techniques for studies of protein-ligand interactions. *Curr. Opin. Struct. Biol. 3*, 760−768.